JOURNAL OF AIRCRAFT
Vol. 30, No. 1, Jan.–Feb. 1993

New Concept in Runback Water Modeling for Anti-Iced Aircraft Surfaces

Kamel M. Al-Khalil*
National Research Council, Washington, D.C. 20418
and
Theo G. Keith Jr.† and Kenneth J. De Witt‡
University of Toledo, Toledo, Ohio 43606

A numerical simulation of the anti-icing of aircraft surfaces is presented. The simulation utilizes the breakup of a uniformly thin liquid film into individual streams or rivulets separated by dry spaces to more accurately describe the physics of runback water. A two-dimensional heat transfer approach is used to calculate the temperature distributions in the runback water and in the solid wall. The model allows a multilayer representation of the solid wall with the possibility of heating the surface by means of electrical heating elements embedded within the layers or by means of convective heating of the surface from the inside using compressor bleed air. Parametric studies are performed to investigate the effects of some of the problem variables on the results.

Nomenclature

A = area
C_p = specific heat
F = wetness factor
g_c = conversion factor
J = mechanical equivalent of heat
h_i = heat transfer coefficient between the hot air and the inner surface of the cowl
h_w = heat transfer coefficient between the outer surface of the cowl and the runback water
h_∞ = heat transfer coefficient between the freestream and the outer surface of the cowl
i, j = x and y grid point locations, respectively
k = thermal conductivity
L_v = latent heat of vaporization of water
m = runback water mass flow rate
m'' = rate of mass transfer per unit area
q = rate of heat transfer
q'' = rate of heat transfer per unit area
q^0 = rate of heat generation per unit volume
R = rivulet radius
T = temperature
w = velocity in a rivulet in the z direction
x, y, z = rectangular coordinates
α = thermal diffusivity
β = collection efficiency or contact angle
δ = maximum height of a rivulet (at $x = 0$)
δ_f = equivalent rectangular film thickness of a rivulet
$\zeta(x)$ = local height of a rivulet
λ = ratio of rivulet width-to-wetness factor, or distance between two adjacent surface streamlines
μ = dynamic viscosity of water
ξ = area correction factor in rectangular film heat loss to ambient
ρ = density
τ = surface shear stress

Subscripts
a = anti-ice air
evap = evaporation from outer cowl surface
imp = impingement on outer cowl surface
m = solid wall composed of several layers
r = rivulet
w = wall or runback water
∞ = freestream

Superscripts
l = layer number in the composite wall
n = Δz step level (grid number in the z direction)

Presented as Paper 91-0266 at the AIAA 29th Aerospace Sciences Meeting, Reno, NV, Jan. 7–10, 1991; received April 13, 1991; revision received Oct. 3, 1991; accepted for publication Oct. 7, 1991.

*NRC Research Associate, NASA Lewis Research Center. Member AIAA.
†Professor, Mechanical Engineering Department. Associate Fellow AIAA.
‡Professor, Chemical Engineering Department.

I. Introduction

TWO conditions are necessary for the formation of structural icing on aircraft surfaces during flight: 1) the aircraft must be flying through visible water, such as rain or cloud droplets; and 2) the surface temperature of the airframe must be below freezing. The detrimental effects of ice buildup are cumulative: the lift coefficient reduces, the drag coefficient increases, and the aircraft weight slightly increases. Furthermore, stall speed of the aircraft increases. The water impinging on the surface can behave in a variety of ways. For example, it may stay in its liquid state if the surface is appropriately heated, and flow downstream where it could entirely or partially wet the surface, totally evaporate, or even freeze if the downstream regions are not thermally protected. In the case where the surface is not continuously heated, the collected droplets may freeze upon impingement and subsequently continue to buildup on the surface until eventually a deicing mechanism must be used for ice shedding. If deicing is accomplished by thermal means, as opposed to mechanical means, the melted water from the interface between the solid surface and the ice can run back and possibly refreeze, creating the so-called "runback" problem.

In a recent study by Al-Khalil et al.,[1] a one-dimensional heat transfer model for the runback water was developed. This model treats the runback water and the solid wall as two separate regions, and the temperature gradient within each domain is assumed to be negligible. The enthalpy transport in the liquid region was taken into account, and a simple phase change model was included to predict the location where the runback water would begin to freeze downstream of the ther-

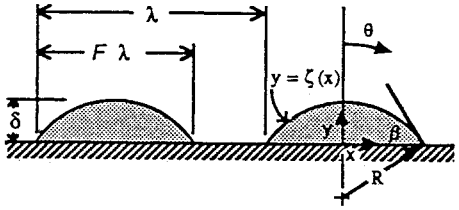

Fig. 1 Rivulet runback model geometry.

mally protected regions. In the present work the model developed in Ref. 1 is referred to as the "basic anti-icing model.

In a later investigation,[2] a model was developed that more accurately represents the surface water behavior. This model was based on an earlier study by Mikielewicz and Moszynski[3] and more recent observations by Hansman et al.[4,5] which include effects of the surface tension phenomenon on the thin liquid water layer. The continuous water layer in the direct impingement region is assumed to form individual, equally spaced rivulets at breakup as shown in Fig. 1. The location of breakup was established based upon the local water film thickness and other operating conditions. The resulting wetness factor and rivulet geometrical properties were also determined.

The present study consists of integrating the concept of rivulets into the analysis of the runback water. This work incorporates the simultaneous heat transfer analysis of the runback water as well as that within the multilayer solid wall over which the water is flowing. This model is herein referred to as the "improved anti-icing model." The results obtained in this study make heavy use of numerical techniques due to the complexity of the conservation equations and the geometries involved.

II. Development of an Improved Model

The basic anti-icing model developed in Ref. 1 was based on a one-dimensional heat transfer formulation. Nevertheless, the model was a major improvement over conventional methods used previously. Despite all of this, a few deficiencies associated with the method were recognized. These included the following:

1) Previous knowledge of the wetness factor is a requirement, either from experiments or from previous experience.

2) The method limits consideration of the wall to be a single layer. In practical applications, the solid wall is composed of several layers within which electrical heating elements may be embeded to provide the required heating for protection against ice buildup.

3) Prior knowledge of the heat transfer coefficient between the solid wall outer surface and the liquid water is required. For this, empirical relations for flow over a flat plate were assumed to be applicable. However, this analogy was found to greatly underestimate those coefficients.

These deficiencies notwithstanding, the model would be a good tool for preliminary design studies. However, a final design study may require an appropriate way of addressing the above issues.

The complete problem that needs to be considered is the simultaneous solution of the temperature distribution of the rivulets and the multilayer solid wall as illustrated in Fig. 2. Generally, the numerical solution of such a problem is very involved. The overall problem requires a simultaneous solution of two governing partial differential equations (PDE). The classification of these PDE's for steady-state conditions are as follows: 1) parabolic in z and elliptic in x and y directions for the rivulet; and 2) elliptic in x, y and z directions in the different layers of the solid wall. Obviously, two three-dimensional problems must be dealt with.

The numerical solution of the equation which governs the rivulet is accomplished using a "marching" procedure in the z direction, i.e., only an initial temperature distribution (at $z = 0$) is required. However, the solution of the solid wall

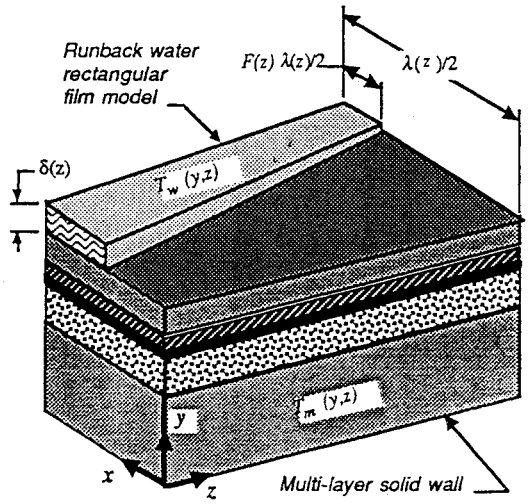

Fig. 2 Rivulet runback model on a multilayer solid wall.

depends on the results of the water temperature distribution along the solid-liquid interface, which are not known a priori. Therefore, an iterative procedure is required in order to satisfy the solid-liquid interfacial thermal boundary conditions—equality of temperature and heat flux balance at the interface between the two regions. These two conditions must be satisfied simultaneously, which adds to the complexity of the problem.

Numerical techniques require the discretization of the solution domain into cells or control volumes that contain nodal or grid points. Generally, the interfacial grid points of the water and the solid wall do not intersect. Moreover, even if they do coincide initially, the rivulet size may eventually decrease due to evaporation as it flows downstream, which causes an alteration in the grid point distribution. This adds a great deal of complexity to the problem since it requires the interpolation of temperatures and heat fluxes at the interface between the water and the solid regions for use in the iterative solution between these two regions. This, in turn, can induce numerical instabilities into the solution procedure, not to mention the substantial amount of computational time that is required. The time was found to increase rapidly with even a modest increase in the number of grid points in the discretized domain of solution. In fact, such a problem does require a large number of nodes for accuracy, for good interfacial interpolation, and for convergence purposes. In order to remedy these problems and to find an appropriate way of modeling the system without jeopardizing the accuracy of the solution, the following two points need to be borne in mind:

1) The temperature distribution within a rivulet, as illustrated in Ref. 2, suggests that the temperature dependence of the rivulet on the y coordinate is much larger than that on the x coordinate.

2) The scales used in drawing the illustration in Fig. 2 are exaggerated. In reality, the size of the rivulet is very small compared with the dimensions of the solid surface. In other words, the thickness of the composite wall (in the y direction) is much larger than its width (in the x direction). Moreover, due to symmetry in the distribution of rivulets on the surface, only half a rivulet and half the dry space between two adjacent rivulets need be considered for the solution. These correspond to insulated boundary conditions at $x = 0$ and $x = \lambda/2$.

These two facts suggest that the temperature variation in the x direction, of the solid wall and the rivulet, is much smaller than that in the y direction. With this in mind, a new rivulet runback model may be introduced which will be called the "rectangular film model." This is shown in Fig. 3. The corresponding representation of the new model of the anti-icing system, referred to as the "improved anti-icing model," is shown in Fig. 4. In this case, the original three-dimensional

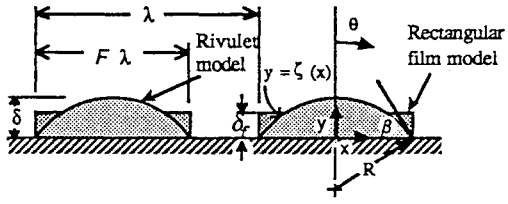

Fig. 3 Suggested rectangular film runback model.

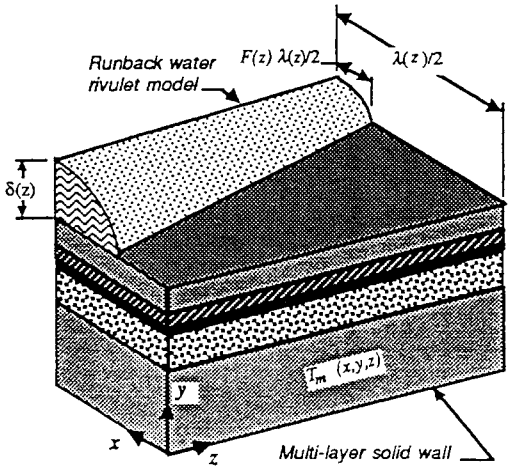

Fig. 4 Rectangular film runback model on a multilayer solid wall.

problem reduces to a two-dimensional problem in both regions (solid wall and liquid water).

The criteria used in the new runback water configuration shown in Fig. 3, are as follows:

1) The wetness factor is taken to be the same in a rivulet and its equivalent rectangular film to preserve the significant behavior of surface water behavior and the physics of the problem.

2) The thickness of the film δ_f is determined by the conservation of mass law. This criterion was chosen because it is the amount of water which runs back that will determine the amount and thickness of ice forming on the surface during a specified time span.

3) Any loss of mass due to evaporation is associated with the decrease in the equivalent rivulet size, i.e., its radius and, consequently, its base width. The reduction in the rivulet width as its base allows the recomputation of a new wetness factor based on the local value of $\lambda(z)$. Then, from the above criterion, the new rectangular film thickness may be recomputed.

III. Mathematical Formulation

A. Runback Water Energy Balance

With regards to the above arguments, and the assumptions made earlier in the thermal analysis of rivulets, the mathematical formulation of the runback water energy equation may be given as

$$\frac{\partial T_w}{\partial z} = \gamma \frac{\partial^2 T_w}{\partial y^2} \tag{1}$$

where

$$\gamma = \frac{\alpha_w}{w(y)}$$

The solution of the above equation requires an initial temperature distribution ($z = 0$), a specified boundary condition at the liquid-gas interface ($y = \delta_f$), and finally, a specified boundary condition at the solid-liquid interface ($y = 0$) which represents the heat exchange between the solid wall and the runback water. The latter boundary condition will be presented later. The boundary condition at the liquid-gas interface is written as

$$-k_w \frac{\partial T_w}{\partial y} = h_\infty (T_w - T_\infty) + m''_{\text{evap}} L_\nu - m''_{\text{imp}} C_{p_w} (T_\infty - T_w) - \frac{m''_{\text{imp}} V_0^2}{2 g_c J} \tag{2}$$

where the first and second terms on the right side of Eq. (2) represent heat loss to the ambient by convection and evaporation, respectively; and the third and fourth terms represent the sensible heat and kinetic energy contributions of the impinging droplets, respectively. The latter two terms are nonzero only in the direct impingement region. The evaporation rate m''_{evap} is the function of the local vapor pressure, relative humidity, and surface temperature. Its calculation procedure is presented in Ref. 1. The rate of impingement depends on the structure geometry, the freestream velocity, and the liquid water content and the droplets size. It is determined from flowfield and water droplet trajectory calculations.

B. Solid Wall Energy Equation

The steady-state heat conduction equation for the different layers in the composite solid surface may be derived by considering a differential control volume of dimensions ($\lambda\, dy\, dz$), and applying the energy conservation law. The solid wall width corresponding to a single rivulet (denoted by λ) as shown in Figs. 3 and 4, is a function of z. This is because it was assumed that each rivulet, upon formation, will flow downstream on the surface following the direction of a surface streamline which is obtained from the flowfield solver. In the case of a two-dimensional body, such as an airfoil, the surface streamlines are parallel. Consequently, λ becomes a constant, that is independent of the z direction. However, if the surface in consideration is, e.g., an engine inlet nacelle, the streamlines are not parallel and λ is not constant.

An energy balance was performed on the control volume mentioned above. The heat conduction equation for the different layers may be readily derived and written as

$$\frac{1}{\lambda(z)} \frac{\partial}{\partial z} \left[\lambda(z) \frac{\partial T_m^l}{\partial z} \right] + \frac{\partial^2 T_m^l}{\partial y^2} + \frac{q^{o l}}{k_m^l} = 0 \tag{3}$$

where $l = 1, 2, \ldots$, number of layers, and $q^{o l}$ is the rate of energy generated per unit volume within layer l and is set equal to the commonly specified heating rate (energy per unit area) divided by the thickness of the corresponding layer of the heating element. This term may be conveniently set to zero except for the active heating element which is modeled as one of the layers in the solid wall. The above formulation assumes constant material properties in each layer.

The boundary condition at the inner surface (lower boundary) of the solid wall, which corresponds to the first layer in the composite surface, may be written as

$$-k_m^l \frac{\partial T_m^l}{\partial y} = q''_{\text{ai}} + h_i (T_a - T_m^l) \quad \text{at} \quad y = 0, \quad \text{and} \quad l = 1 \tag{4}$$

where q''_{ai} is a specified anti-icing heat flux applied to the inner surface of the wall, and the second term on the right side of the equation represents the convective heating of the inner surface in the case where the anti-icing system relies on compressor bleed air. In addition, either q''_{ai} or h_i may be set to zero, depending on which case is being considered, or both may be set to zero for the case where the inner surface is perfectly insulated.

The boundary conditions that must be satisfied at a solid-solid interface between layers "l" and "$l + 1$," are

$$T_m^l = T_m^{l+1} \tag{5}$$

$$k_m^l \frac{\partial T_m^l}{\partial y} = k_m^{l+1} \frac{\partial T_m^{l+1}}{\partial y} \tag{6}$$

As to the boundary condition on the left side ($z = 0$) and the right side of each layer, it may be either one of the following: a specified temperature distribution (if its prediction is possible), or an insulated boundary.

Finally, the boundary conditions that remain for the simultaneous solution of Eqs. (1) and (3) are those relating to the solid-liquid interface. These correspond to the interface between the runback water and the outermost (upper) layer in the wall, and they may be written as follows:

$$T_m^l = T_w \text{ (equal temperatures at solid-liquid interface)} \tag{7}$$

$$-k_m^l \frac{\partial T_m^l}{\partial y} = -k_w F \frac{\partial T_w}{\partial y} + h_\infty(1 - F)(T_m^l - T_\infty) \tag{8}$$

In the above pair of equations, l represents the outermost layer. Equation (8) simply states that heat is transferred from the solid surface proportionally through the wetted (to the runback water) and the dry (to the ambient) surface areas of the wall.

IV. Numerical Solution Methods

Due to the existence of the highly nonlinear governing equations, an analytical solution to the problem becomes virtually impossible. On the other hand, the use of numerical techniques which are suitable for execution on a digital computer is quite appropriate. Details of the solution procedure were omitted due to the lack of space but are fully presented in Ref. 6. However, a brief description of the methods is provided in the following sections.

A. Runback Water

The numerical solution of the runback water energy equation, given by Eq. (1), was carried using a fully implicit scheme. The method is unconditionally stable and is described in Ref. 7. It employs a backwards finite difference for gradients in the z direction, and a central difference for gradients in the y direction. Consequently, the finite difference representation of Eq. (1) may be written as follows:

$$\frac{T_j^{n+1} - T_j^n}{\Delta z} = \gamma_j \left(\frac{T_{j+1}^{n+1} - 2T_j^{n+1} + T_{j-1}^{n+1}}{\Delta y^2} \right) \tag{9}$$

where the superscript n represents the grid number in the z direction, and the subscript j denotes the node number in the y direction. The set of equations corresponding to the various nodes may be rearranged in a tridiagonal matrix form. This allows one to take advantage of the high speed Thomas Algorithm solver.[7]

In addition to the above equations, two equations are still required before performing the simultaneous solution of the linear equations. These difference equations are derived from the boundary conditions given by Eqs. (7) or (8), and Eq. (2), respectively. For this, Eq. (8) was used in the solution of the runback water energy equation, while Eq. (7) was used in the solution of the outermost layer in the solid wall.[6] The resulting finite-difference equations become

$$-T_{M-1}^{n+1} + \left[1 + \frac{\Delta y}{k_w} (h_\infty \xi + m''_{\text{imp}} C_{p_w}) \right] T_M^{n+1} = \frac{\Delta y}{k_w} \left[(h_\infty \xi + m''_{\text{imp}} C_{p_w}) T_\infty - m''_{\text{evap}} L_v \xi + \frac{m''_{\text{imp}} V_0^2}{2 g_c J} \right] \tag{10}$$

where M is the node number at the liquid-gas interface, and

$$\left[1 + \frac{h_\infty(1 - F)\Delta y}{F k_w} \right] T_1^{n+1} - T_2^{n+1} = \frac{\Delta y}{F k_w} [q''_m + h_\infty T_\infty (1 - F)] \tag{11}$$

Note that ξ in Eq. (10) is an area correction factor to account for the area differences in the rivulet and the rectangular film models through which heat exchange with the ambient air occurs. This factor is defined as the ratio of the rivulet-free surface area to the upper surface area of the corresponding rectangular film. From geometric considerations, ξ may be shown to be equal to $\beta/\sin\beta$. This factor is close to unity for small-to-moderate contact angles, and is unity for uniform film flow.[6] The heat flux q''_m in Eq. (11) is computed numerically from the temperature distribution in the solid wall at the solid-liquid interface. Since the solution procedure for the combined water/solid wall problem is iterative, it is assumed in the above equations that a temperature distribution in the solid already exists from the previous iteration.

A relation between a rivulet radius and its corresponding rectangular film thickness may be written as[6]:

$$\delta_f = R \sqrt{\frac{F_1(\beta)}{\sin\beta}} \tag{12}$$

where the function $F_1(\beta)$ was derived in Ref. 2. Also, relations for the film thickness between two consecutive Δz steps were developed:

$$\delta_f^{n+1} = \delta_f^n \left[1 + \frac{2R\beta\Delta z(m''_{\text{imp}} - \xi m''_{\text{evap}})}{m_r^n} \right]^{1/3} \quad (F < 1) \tag{13}$$

$$\delta_f^{n+1} = \sqrt{\delta_f^{n} + \frac{2\mu\Delta z}{\rho\tau}(m''_{\text{imp}} - m''_{\text{evap}})} \quad (F = 1) \tag{14}$$

B. Solid Wall

The governing PDE given by Eq. (3) was derived by applying the conservation of energy law on a differential control volume. However, in an attempt to write the finite-difference representation of this equation, the conservative properties of the equation may be lost depending on how the derivatives are approximated. This may lead to the existence of small artificial heat sources or sinks in the numerical solutions. This point may be visualized by considering the finite-difference representation corresponding to an internal node in a particular layer. The nodal temperature is seen to depend on the temperatures of the four neighboring nodes. However, at a solid-solid interface, the temperature of an interfacial node depends only on the two neighboring nodes in the y direction when a direct finite-differencing is applied to the boundary condition described by Eq. (6). However, in the control volume approach, the fact that conduction may occur along the nodes in the x direction is recognized and is taken into account.

The control volume approach has the distinctive characteristic that a balance of the specific physical quantity, whether it is mass, momentum, or energy, is achieved in the cell (volume) of a grid point. Thus, this approach was used in the formulation of the difference equations rather than directly approximating the governing and boundary conditions by finite differences. Consequently, finite-difference equations were developed for the various types of nodes that exist in the composite wall. These nodes may be classified as one of the following: 1) an internal node within a particular layer, 2) a side node, 3) a corner node, or 4) an interfacial node (internal and side). Further details are presented in Ref. 6.

C. Numerical Solution Procedures

The simultaneous solution of the energy equations for the runback water and for the solid wall layers requires an iteration procedure. The boundary conditions that must be satisfied at the solid-liquid interface are those of equal temperature and the balance of heat fluxes given by Eqs. (7) and (8), respectively. One of these boundary conditions must be used in the runback water solution procedure and the other in the solid wall solution procedure.

Initially, it was planned to use Eq. (7) in the water solution and Eq. (8) in the wall solution. In other words, the most recent solid wall temperature distribution at the outer surface is used as the lower boundary condition in the water solution. However, this technique was found to be highly unstable because the solid wall was very sensitive to heat flux values calculated from the right side of Eq. (8), which uses the most recent temperature distribution in the water. To remedy this problem, an underrelaxation factor was used in the following manner: only a small specified percentage of the computed change in the value of the right side of Eq. (8) between two consecutive iterations is added to the value from the previous iteration. The value of the underrelaxation factor depends on the particular problem conditions. Its effect is to smoothly and slowly drive the computed results towards the actual solution in a stable manner. However, this method failed to work due to instabilities, even for very small underrelaxation factors. The problem was resolved by switching the interfacial boundary conditions between the runback water and the solid wall. Nevertheless, an underrelaxation factor was still needed.

The steps followed during the iterative solution procedure of the combined runback water and solid wall problem are listed in order as follows:

1) Compute the heat flux at the solid-water interface corresponding to the solid wall nodes using a local one-dimensional heat transfer approach, i.e., neglect conduction within the wall in the z direction. To get the iterative procedure started, the outer wall surface is assumed to be free of runback water. It was also assumed that, for the first iteration, any heat generated within the wall layers is transferred in the external direction to the ambient air.

2) Solve for the runback water temperature distribution $T_w(y, z)$ using the computed heat flux values following the marching procedure described earlier.

3) Interpolate the solid wall interfacial temperature values T_m from those of the runback water calculated in the preceding step, using a cubic spline interpolation technique. Also, set up the convective boundary condition for the dry region of the outer wall surface in case total evaporation of the runback water occurs.

4) Solve the linear system of equations corresponding to the solid layers and obtain the temperature distribution.

5) Recompute the solid wall interfacial heat flux from the most recently computed solid wall temperature distribution, and then, using the cubic spline procedure, interpolate for the corresponding values of the runback water interfacial nodes.

6) Recompute the runback water temperature distribution $T_w(y, z)$ as in step 2.

7) Interpolate values of T_m at the outer wall surface as in step 3, and set up the convective boundary conditions in the dry region.

8) Solve for $T_m(y, z)$.

9) Compare values of $T_m(y, z)$ at several nodes with the corresponding values of the previous iteration. If the convergence criteria is satisfied the steady values of the runback water and solid wall temperature distributions are those obtained in the last iteration. Otherwise, reset values of all the variables to their initial values (at $z = 0$), and perform another iteration starting from step 5. This process is repeated until convergence of the solutions is met.

In steps 2 and 6, the film thickness should be updated after each Δz step in the marching procedure using Eqs. (13) and (14). Also, if the uniform film thickness falls below the critical film thickness at, or downstream of, the impingement limit as described in the previous paper,[2] the film breaks up into identical rivulets whose radii are updated after each step Δz of the solution. The value of the critical film thickness depends on the liquid properties (viscosity, density, and surface tension), the contact angle β, and the wall shear stress τ obtained from the viscous flowfield solution. An updated wetness factor is subsequently obtained from geometric considerations and mass conservation between the rectangular film and its equivalent rivulet of same base width (i.e., both have the same wetness factor.)[2] The latter reference contains a detailed explanation of this approach. It was assumed that the direct impingement region is fully wetted as the result of the continuous impingement of water droplets. In the case of very large impingement rates, such as rain, the film remains continuous for a long distance. However, in aircraft icing applications the rate of runback water flow on the surface is generally relatively small. This leads to small flow rates and consequently small film thicknesses which may become unstable and breakup into rivulets.

V. Sample Results and Discussion

In the following, two example problems will be considered in order to demonstrate the numerical calculation procedure. The purpose of the first example is to compare the basic and the improved anti-icing models. In the second example, the flow of the thin water layer over a heated composite body is considered. This also involves a parametric study of some variables to demonstrate their effects on the solution.

A. Example 1

Consider liquid water droplets impinging on the leading edge of an airfoil surface such that the distribution of the impingement rate is as shown in Fig. 5, where z is the wrap distance from the stagnation point. The impingement limit is the location where the rate of water impingement becomes zero; in this case, it is at $z = 0.25$ m. The surface is assumed to be heated on the interior by means of convection from hot air whose temperature varies linearly from 220°C at $z = 0$ to 120°C at $z = 0.5$ m. The distribution of the external heat transfer coefficient between the ambient air and the outer surface, and the internal heat transfer coefficient between the hot anti-icing air and the inner surface, are shown in Figs. 6 and 7, respectively. The solid wall is assumed to be composed of a single metal layer whose thermal conductivity is 100 W/m K. The ambient conditions are taken to be $T_\infty = -10$°C, $P_\infty = 0.5$ atm, and the relative humidity is 100%. The runback water flow is assumed to be due to a shear force with a value of $\tau = 10$ Pa acting on the free surface; and the contact angle of the rivulets, if breakup of the film occurs, is $\beta = 40$ deg.

In the basic anti-icing model, the heat transfer coefficients between the solid wall and the runback water were computed using flat plate theory. On the other hand, average Nusselt numbers were computed for rivulet flow.[6] The Nusselt number corresponding to a thin film flow was found to be equal to 2. In the following calculations results of the flat plate

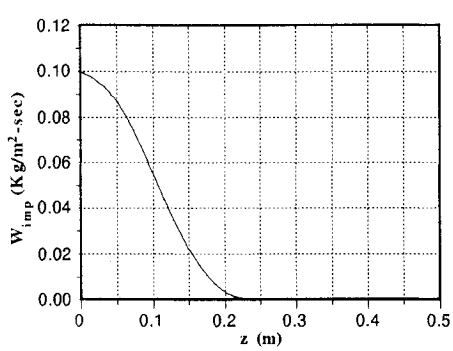

Fig. 5 Rate of water impingement per unit area.

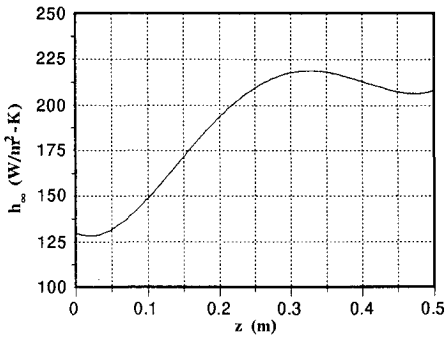

Fig. 6 External heat transfer coefficient.

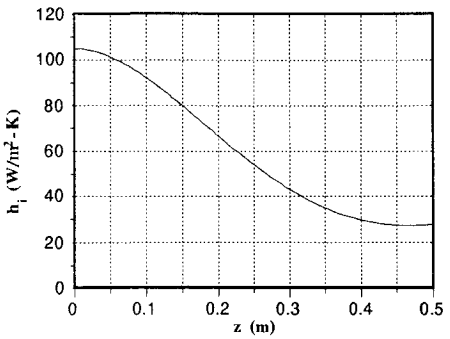

Fig. 7 Internal heat transfer coefficient.

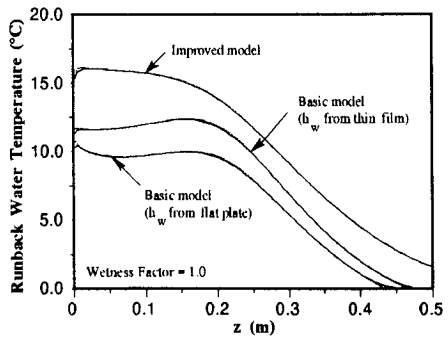

Fig. 8 Average runback water temperature distribution for the models at $F = 1.0$.

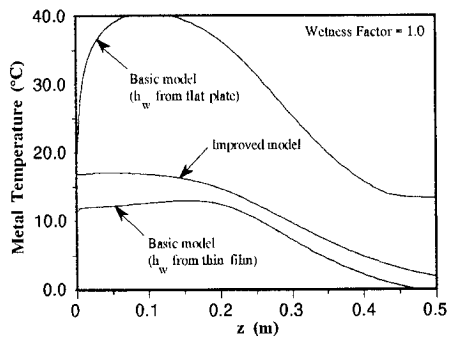

Fig. 9 Average metal temperature distribution for the models at $F = 1.0$.

theory as well as the thin film theory in the basic anti-icing model will be presented when comparing results along with those of the improved anti-icing model.

Consider the case where the wetness factor is unity across the entire surface. The corresponding results for the runback water temperature, the metal temperature, and the film thickness are shown in Figs. 8, 9, and 10, respectively. It should be noted that the temperatures in the case of the improved model are averaged over the transverse direction from the two-dimensional solution. It is clear that the thin film theory

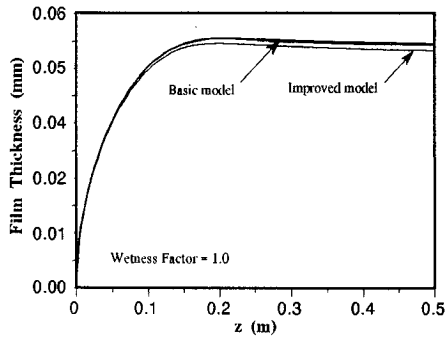

Fig. 10 Film thickness distribution at $F = 1.0$.

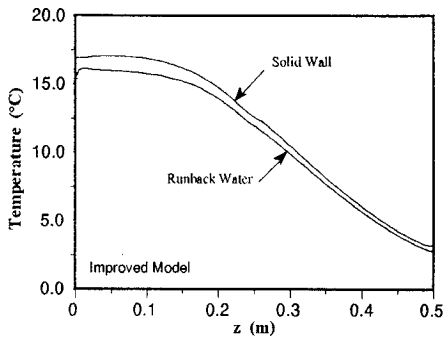

Fig. 11 Average water and metal temperature distributions for the improved model.

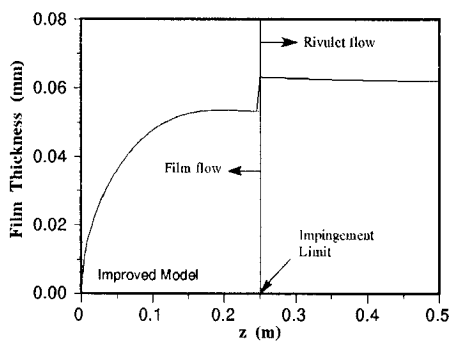

Fig. 12 Film thickness for the improved model.

is far better than the flat plate theory since the results are closer to those of the improved model. This is substantiated by Fig. 9 which shows the metal temperature distributions. It is assumed that the improved model offers the more accurate mathematical solution to the problem since it does not require knowledge of the heat transfer coefficient at the solid/liquid interface. In fact the latter is calculated from the resulting two-dimensional temperature distributions. The discrepancy shown in the results of Fig. 9 is due to the fact that the heat transfer coefficients calculated from the flat plate theory are at least two orders of magnitude smaller than those calculated from the thin film theory. However, as shown in Fig. 10, good agreement between the predicted values is found for the film thickness, which is directly related to the water mass flow rate, in all the models considered.

During the numerical solution of the improved model, it was observed that, based on the critical film thickness,[2] the water film would breakup into individual rivulets at the impingement limit. However, this fact was overridden in the computer code for the above example, and the wetness factor was forced to have the value of unity for comparison purposes with the basic model. Nevertheless, if the film is allowed to breakup as it is supposed to, the corresponding results of the improved model are shown in Figs. 11–13. Figure 13 shows that the film breaks up at the impingement limit because the

Table 1 Composite wall physical and thermal properties

Layer no.	Description	Material	Thickness, mm	Thermal conductivity, W/m.K
1	Substrate	Aluminum alloy	2.20	220
2	Inner insulation	Epoxy/glass	1.30	1.25
3	Heater[a]	Copper	0.20	340
4	Outer insulation	Epoxy/glass	0.25	1.25
5	Abrasion shield	Stainless steel	0.30	50

[a]Heater power density = 7.74 W/in.^{2}

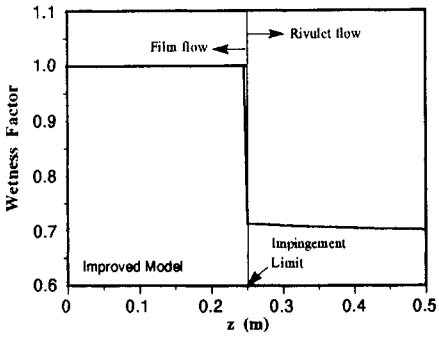

Fig. 13 Wetness factor for the improved model.

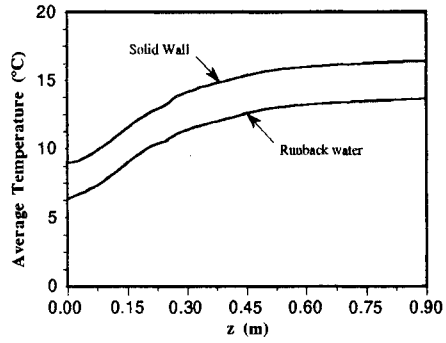

Fig. 14 Water and solid wall average temperature distributions.

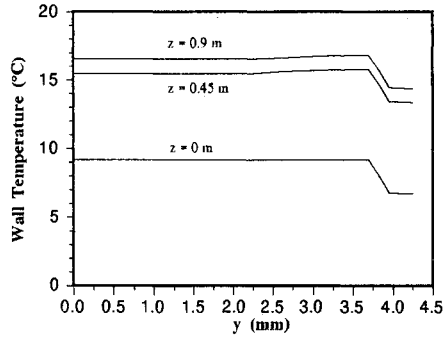

Fig. 15 Wall temperature distribution in the y direction at several z locations.

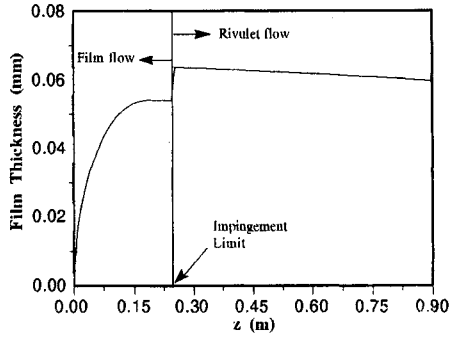

Fig. 16 Film thickness distribution.

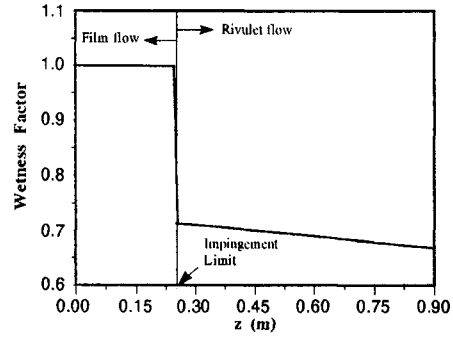

Fig. 17 Wetness factor distribution.

local film thickness is below the critical film thickness.[2] Since the breakup of the film produces dry spaces between adjacent rivulets, the film thickness increases at the impingement limit (as shown in Fig. 12) and then decreases slowly due to evaporation losses.

Additional results are available in Ref. 6. The effect of the wetness factor on the temperature distributions was investigated. A decrease in the wetness factor leads to a decrease in the surface area of the water film which is exposed to the ambient. Consequently, the potential of heat loss to the ambient by convection and evaporation is reduced. Obviously, this drives the water temperature up. The evaporation process is very significant due to the large value of the water latent heat. Therefore, an accurate evaluation of the wetness factor is crucial.

B. Example 2

The next example considers the case in which the solid wall is composed of five layers, similar to the illustration in Fig. 4. The physical and thermal properties of these layers are presented in Table 1. The layers are numbered in an ascending order starting from the innermost layer and progressing to the outermost layer. The wall configuration considered is typical of some aircraft surfaces and helicopter rotor blades. The middle layer is an electrical heating element and serves as the heat source that is used to maintain the outer surface free from ice and to prevent the runback water from freezing.

The ambient conditions are the same as those in the preceding example, except that the air inside the airfoil is held at ambient conditions, i.e., at a temperature of -10°C. The heat transfer coefficient at the inner surface is assumed to be due to free convection and is taken to have a constant value of 10 W/m^2.K. The length considered along the outer surface in the z direction is 0.9 m. Results for this case using the improved anti-icing model are presented in Figs. 14–17.

Figure 14 illustrates the average temperatures of the solid wall and the runback water. The temperature difference between the two is approximately constant (approximately 2.7°C). This is due to the fact that the film thickness is very small, and therefore, rapidly responds to the environmental conditions. The temperature distribution within the solid layers are plotted in Fig. 15 at three different z locations. The largest temperature gradients occurred in the layers of least thermal conductivity, layers 2 and 4, as expected. Even though the thickness of layer 4 is about one-fifth of layer 2, a smaller drop occurred in the latter due to the fact that the heat transfer

coefficient at the inner surface of the wall is much smaller than that at the outer surface. This causes most of the heat generated in the heater (layer 3) to flow towards the surface water. In fact, it was found that the ratio of the rate of heat flowing towards the water-solid interface to the heat flowing towards the internal air-solid interface from the heater element is on the order of the ratio of the external to internal heat transfer coefficients.

Figures 16 and 17 are plots of the film thickness and the wetness factor, respectively. As shown, the uniform film broke up into rivulets at the impingement limit. In downstream regions, the film thickness and the corresponding wetness factor are seen to decrease slowly, in a linear fashion. This was found to be always true except when the rivulet (rectangular film) approached total evaporation, as will be shown next.

The effects of the heater power density on the runback water temperature distribution, film thickness, and wetness factor are illustrated in Figs. 18, 19, and 20, respectively. These figures demonstrate that total evaporation of the runback water may be accomplished by increasing the heater power output. Any further increase of power density (beyond the values shown) causes evaporation of the runback to occur at shorter distances, as is expected. It is interesting to note that the film thickness decreases in a nearly linear manner up to a particular location where the film thickness, as well as

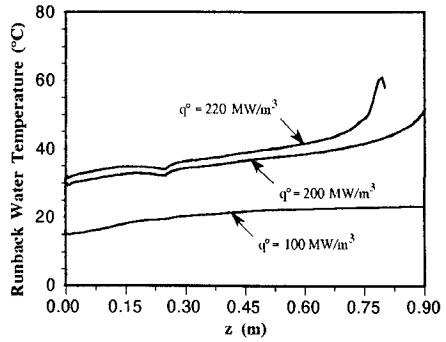

Fig. 18 Average water temperature distributions at various heater power densities.

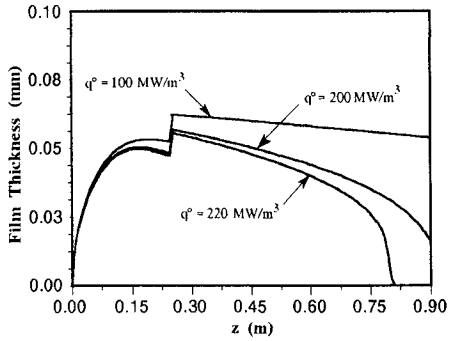

Fig. 19 Film thickness distribution at various heater power densities.

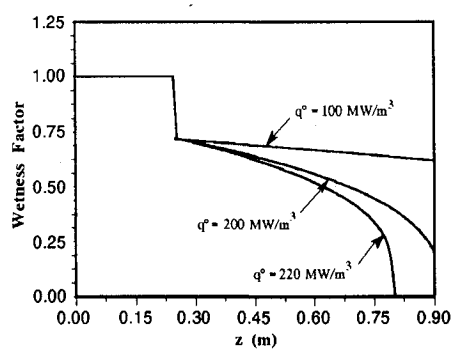

Fig. 20 Wetness factor distribution at various heater power densities.

the wetness factor, decreases rapidly until total evaporation is accomplished. The slope in the linear decrease region depends principally on the external heat transfer coefficient, on the local ambient pressure, and on the humidity conditions. The thickness corresponding to the location where the slope starts increasing rapidly depends mostly on the net rate of heat supplied to the runback water.

The effect of the magnitude of the shear force imposed on the liquid-free surface was not excluded in this study. It was found that the shear force has no significant effect on the average water temperature distribution and the wetness factor, and it only affects the film thickness since for a given flow rate the thickness decreases when the average velocity increases due to an increase in τ.[6] However, the largest effect of the wall shear force occurs when the water temperature reaches 0°C. More ice would form when the shear force is small due to the magnitude of the film average speed.

A two-dimensional phase change model was found to be inappropriate in the improved model. The surface at the outer edge of the film has the lowest temperature within the film cross section, and therefore, has the tendency to freeze first causing a complex behavior of the water flow and its freezing. Since the temperature drop across the film thickness is small, it may be assumed that the phase change model developed in the basic anti-icing model[1] applies in this case when the average temperature of the liquid runback water reaches the value of 0°C. Since the temperature was lumped over the y direction in the basic model, it was assumed that the water would remain in its liquid state at 0°C until it gives up all of its latent heat of fusion, and then suddenly turn to solid ice at a downstream location. However, it is recommended that as soon as the runback liquid water temperature reaches 0°C, any further loss of its latent heat is associated with the freezing of a fraction of the runback water. This may be taken to be proportional to the ratio of the heat loss value to the total latent heat value.

The contact angle in a rivulet depends on the properties of the involved media. The effect of the magnitude of the contact angle on the results was examined.[6] For a given mass flow rate and, consequently, film thickness at the impingement limit, the wetness factor and the resulting film thickness after breakup are only slightly affected by the contact angle in the case where breakup occurs at the impingement limit, which is most likely in aircraft icing problems due to the limited collection of water. The effect of a decrease in the contact angle is to slightly increase the runback water average temperature because of the decrease in the actual rivulets dimension.

VI. Concluding Remarks

Additional parametric studies are possible, and the results are dependent on the particular ambient conditions, the anti-icing system, the physical properties, and the structure of the solid wall. Due to the large number of variables involved in the problem, even if only slight changes in each variable had a small effect on the results, the overall effect of the variables may be significant on the final results.

As far as the accuracy of the numerical results is concerned, the solution was considered accurate for several reasons.[6] Unfortunately, experimental validation of the model was not possible at the time this study was performed. However, the model may be used as a tool for determining a set of experimental conditions that may be effectively used in the validation of the computer code. The code may also be used as a tool for designing new anti-icing systems or modifying existing systems.

Acknowledgments

The present investigation was sponsored by the General Electric Company, William South, grant monitor, the continuous support of this work is gratefully acknowledged. Also, several cases were run on the Cray Y-MP at the Ohio Super

Computer Center; the use of the supercomputer is appreciated.

References

[1]Al-Khalil, K. M., Keith, T. G., De Witt, K. J., Nathman, J. K., and Dietrich, D. A., "Thermal Analysis of Engine Inlet Anti-Icing Systems," *Journal of Propulsion and Power*, Vol. 6, No. 5, 1990, pp. 628–634.

[2]Al-Khalil, K. M., Keith, T. G., and De Witt, K. J., "Development of an Anti-Icing Runback Model," AIAA Paper 90-0759, Reno, NV, Jan. 1989.

[3]Mikielewicz, J., and Moszynski, J. R., "Breakdown of a Shear Driven Liquid Film," Polish Academy, Prace Instytutu Maszyn Przeplywowych, No. 66, 1975, pp. 3–11.

[4]Hansman, R. J., and Turnock, S. R., "Investigation of Surface Water Behavior During Glaze Ice Accretion," *Journal of Aircraft*, Vol. 26, No. 2, 1989, pp. 140–147.

[5]Hansman, R. J., Yamaguchi, K., Berkowitz, B., and Potapczuk, M., "Modeling of Surface Roughness Effects on Glaze Ice Accretion," AIAA Paper 89-0734, Reno, NV, Jan. 1989.

[6]Al-Khalil, K. M., "Numerical Simulation of an Aircraft Anti-Icing System Incorporating a Rivulet Model for the Runback Water," Ph.D. Dissertation, Univ. of Toledo, Toledo, OH, Dec. 1990.

[7]Anderson, D. A., Tannehill, J. C., and Pletcher, R. H., *Computational Fluid Mechanics and Heat Transfer*, Hemisphere, New York, 1984, pp. 55–63.